Proceedings of the 9th U.S. National and 10th Canadian Conference on Earthquake Engineering
Compte Rendu de la 9ième Conférence Nationale Américaine et
10ième Conférence Canadienne de Génie Parasismique
July 25-29, 2010, Toronto, Ontario, Canada • Paper No 746

BEHAVIOR OF HIGH-PERFORMANCE FIBER-REINFORCED CEMENTITIOUS COMPOSITE MATERIALS FOR EARTHQUAKE-RESISTANT DESIGN

R. R. Foltz[1] and J. M. LaFave[2]

ABSTRACT

Development and modeling of High Performance Fiber-Reinforced Cementitious Composites (HPFRCC) for use in key shear and/or moment regions of damage-critical concrete structural elements is currently being investigated. More specifically, HPFRCC is being explored for use in the coupling beams of coupled shear walls, a popular reinforced concrete (RC) structural system for medium-rise structures in areas of moderate to high seismicity, as well as in the plastic hinging regions of the structural walls themselves. An experimental program has been conducted to further understand the behavior of HPFRCC under general biaxial stress states, such as would be expected at various key locations in a coupling beam. Concrete plate specimens comprising mixes containing from one to two percent volume fraction of hooked steel fibers and Spectra (polyethylene) fibers have been tested. After exploration of these different fiber types and volume fractions, a 1.5 percent volume fraction of hooked steel fibers was selected as the concrete mix for more comprehensive examination. HPFRCC in compression was found to exhibit about 50 percent residual stress up to 0.03 strain, as well as a shift in failure mechanism from tensile splitting to faulting or shear failure. Also, the strength envelope shows biaxial compressive strength gains of over 40 percent with the addition of HPFRCC. Using the knowledge and behavioral trends gained from the laboratory tests of these HPFRCC materials, it can be possible to extrapolate their energy dissipating behavior to uses in structural elements for seismic design.

Introduction

Interest in development of high-performance fiber-reinforced cementitious composites (HPFRCCs) as a design alternative to alleviate reinforcement congestion in critical shear and/or moment regions of reinforced concrete coupled shear walls has been considered. Use of HPFRCC may allow for simplified reinforcement detailing with adequate damage tolerance through a ductile response obtained by the tensile strain-hardening and confined compressive behavior of the material. Thus, use of HPFRCC materials in large-scale structural applications could significantly reduce the amount of reinforcement required to ensure adequate performance

[1]Graduate Research Assistant, Dept. of Civil and Environmental Engineering, University of Illinois at Urbana-Champaign, Urbana, IL 61801
[2]Associate Professor, Dept. of Civil and Environmental Engineering, University of Illinois at Urbana-Champaign, Urbana, IL 61801

in areas of inelastic deformation demands, while also potentially reducing labor costs and construction time delays (Parra-Montesinos 2005). Due to increased costs associated with using HPFRCC, the material has been targeted for critical regions where substantial reinforcement detailing is required for adequate behavior during earthquakes. Canbolat et al. (2005) investigated the use of HPFRCC coupling beams without transverse reinforcement around the main diagonal reinforcing bars – results indicated that a reduction in reinforcement may be achieved in HPFRCC coupling beams without compromising the shear strength, due to the additional diagonal tensile strength provided by the fibers. Since cast-in-place HPFRCC coupling beams could present constructability issues, using precast HPFRCC beams in combination with conventional reinforced concrete structural walls has been proposed.

The experimental program reported here has been conducted to further understand the behavior of HPFRCC under general uniaxial and biaxial stress states (such as would for instance be expected at various key locations in a coupling beam). Concrete plate specimens comprising mixes containing from one to two percent volume fraction of hooked steel fibers or Spectra (polyethylene) fibers were tested under uniaxial and biaxial compression, and failure envelopes were developed for each type of concrete. Although the experiments were not conducted cyclically, their results (developing monotonic nonlinear material behaviors) can be implemented in conjunction with a damage rule for subsequent modeling of material and structural behavior under cyclic loading. Previous test results revealed that, across both fiber types the residual strength during uniaxial testing exceeded 60 percent of the maximum stress at as much as 2 percent strain, with the level of residual strength depending on the fiber volume fraction. Under equal biaxial compression a strength increase of greater than 50 percent over the uniaxial value was observed for both fiber types (Foltz et al. 2008). An even more comprehensive experimental examination is underway for a 1.5% volume fraction mix with hooked steel fibers. Failure envelopes have been developed for each type of composite, and their stress-strain behaviors as well as failure mechanisms were observed. Currently, the full range of compressive biaxial behavior of HPFRCC has been examined; future tests will also explore tensile stresses. Using the observed HPFRCC behavioral trends, it will be possible to extrapolate the energy dissipating behavior to some potential seismic design and construction applications.

Experimental Program

Experimental Overview

Hooked steel fiber, Spectra fiber, and plain concrete mixes were investigated. (The Spectra fibers are strong and durable white polyethylene fibers made by Honeywell.) The mixes were first cast as individual 5.5 x 5.5 x 1.5 in. (140 x 140 x 38 mm) specimens, a size similar to historical concrete biaxial tests (Kupfer et al. 1969). Three concrete mixtures were explored, the Mortar Mix (MM), NEES Mix #4 (NM4), and NEES Mix #6 (NM6) (Liao et al. 2006). Specimens were cast with Spectra fibers, hooked steel fibers, or without fibers for the MM, while only hooked steel fiber and plain concrete mixes were batched for NM4 and NM6. To explore the influence of specimen type on orientation of the fibers (and therefore on biaxial behavior), large 6.5 x 6.5 x 18 in. (165 x 165 x 457 mm) loaves of the MM were also cast (to ensure a random orientation of the fibers). These loaves were then cut and trimmed to the aforementioned specimen size using a diamond precision saw. Upon visual inspection, it was clear that the fibers were randomly well-dispersed in the loaf specimens. The first generation of tests utilized the MM and NM4 designs, with their results (comparing individually cast specimens to loaf

specimens) influencing the decision to explore only casting in loaves for the eventual NM6 design (Foltz et al. 2008). For the MM specimens, 1.0, 1.5, and 2.0 percent fiber volume fractions were used for both fiber types, while only a 1.5 percent hooked steel fiber volume fraction was used for the NM4 and NM6 specimens. Table 1 displays the testing specimen matrix. In addition to the plate specimens, 15 NM6 4 x 8 in. (102 x 203 mm) cylinder specimens were cast and tested for comparison with the plate uniaxial compression results.

Table 1.   Specimen testing summary.

Mix	Specimen Type	Fiber Type	Average Uniaxial Plate Compressive Strength, ksi (MPa)	Total Number of Specimens
Mortar Mix	Individual	Hooked	10.2 (70.1)	30
		Spectra	8.7 (60.2)	21
		Plain	8.6 (59.4)	9
	Loaf	Hooked	6.6 (45.8)	17
		Spectra	5.8 (39.9)	18
NEES Mix #4	Individual	Hooked	6.3 (43.6)	28
		Plain	7.6 (52.7)	10
NEES Mix #6	Loaf	Hooked	4.9 (33.5)	20
		Plain	5.4 (37.3)	12

All test specimens were made using Type III Portland cement; Table 2 displays the proportions of each mix by weight of cement. The coarse aggregate used in NM4 and NM6 had a maximum aggregate size of ½ in. (13 mm), and the fine aggregate for both mixes was #16 flint silica sand supplied by the U.S. Silica Company. The hooked steel fibers were Dramix® RC-80/30-BP with a length of 1.2 in. (30 mm), a diameter of 0.015 in. (0.38 mm), and a tensile strength of 334 ksi (2300 MPa). The Spectra® fibers had a length of 1.5 in. (38 mm), a diameter of 0.0015 in. (0.038 mm), and a tensile strength of 375 ksi (2580 MPa).

Table 2.   Mixture proportions by weight of cement.

Matrix Type		Mortar Mix	NEES Mix #4	NEES Mix #6
Cement – Type III (Early Age)		1	1	1
Aggregates	**Silica Sand (Flint)**	1	2.5	2.2
	Coarse Aggregate	–	1.25	1.2
Fly Ash – Class C		0.15	0.875	0.875
Chemical Admixtures	**Super-Plasticizer**	–	0.0055	0.005
	VMA	–	0.065	0.038
Water		0.4	0.84	0.8
Fibers	**Types of Fibers**	Hooked, Spectra	Hooked	Hooked
	Percent Volume Fraction	1.0, 1.5, & 2.0	1.0, 1.5, & 2.0	1.5
28-Day Compressive Strength, ksi (MPa)		8 (55.2)	5.1 (35.2)	5.5 (37.9)

The mixing protocol outlined by Liao et al. (2006) was followed when batching the specimens (under the supervision of project partner colleagues at the University of Michigan).

During the addition of fibers, special care was made to ensure that they did not clump, especially for the Spectra fibers. Once the specimens were cast into a plastic mold, they were placed on a vibrating table to achieve sufficient compaction. After each pour, specimens were kept in their molds and covered with plastic sheets for about 24 hours. They were removed from the molds and placed into a water curing tank for at least another 28 days. All specimens were allowed to dry for at least 48 hours prior to testing. As previously noted, specimens cast as loaves were cut with a diamond precision saw to 5.5 x 5.5 x 1.5 in. (140 x 140 x 38 mm). To ensure uniform biaxial stress and strain fields, the four sides of each specimen were then ground to achieve flat edges and right-angle corners. A problem encountered during some testing was local damage at the interface between the specimen and the platen; however, trimming the edges of the specimens to avoid areas where the strength may be lower due to bleeding proved to be effective.

The experiments were displacement controlled, with the ratio of principal strains varied in an effort to obtain a comprehensive understanding of the biaxial material behavior. Testing was conducted using a 112 kip (500 kN) INSTRON biaxial servo-controlled hydraulic frame. A closed-loop system in displacement control was used to capture the post-peak response of the specimens, and all biaxial compressive loads were applied simultaneously. Displacement control was provided by AC linear variable differential transducers (LVDTs) attached to the hydraulic actuators. Each axis of loading had one actuator slaved to a master actuator through digital line connections. The closed-loop control of the actuators was executed using INSTRON 8500 / 8800 controllers. Similar to previous researchers (Kupfer et al. 1969, Nelissen 1972, etc.), frictional confinement of the test specimens by the loading platens was minimized by using brush-type loading platens. The brush platens were pin-connected to the fixtures (including simple guide-ways to ensure planar loading), which were in turn mounted on the load cell of each actuator. For compression (and equal biaxial compression), the standard applied strain rate was 0.01 in./min. (0.25 mm/min.). For intermediate targeted stress ratios, the standard applied strain rate was simply reduced in the horizontal direction to try to achieve the desired stress ratio.

Strain and displacement measurements were obtained using the non-contact Krypton K600 Dynamic Measuring Machine (DMM), which can obtain the three-dimensional location of small light-emitting diodes (LEDs) to an accuracy of +/- 0.0008 in. (0.02 mm) at a sampling rate of up to 1000 readings per second. For these tests, LEDs were placed on an overall 3 in. x 3 in. (75 mm x 75 mm) grid (with 1.5 in. spacings) centered on the specimen. To obtain additional out-of-plane data, two 0.25 in. (6 mm) stroke LVDTs were positioned on special frames and placed such that they were touching the center of each face of the specimen, as shown in Figure 1. (Early tests were conducted using 9 LEDs on the front of the specimen, with a single LVDT at the center of the back of the specimen; however, it was later found that the out-of-plane data was less noisy when two LVDTs were used.) Analog output signals from the measuring devices were connected to input channels of the data acquisition system. Four-axis control of the system was synchronized with a PC using Labview, allowing synchronization of the start of each test, as well as of the load, displacement, and LVDT data collection. Several two-axis plots were displayed with real-time updates to monitor performance and behavior of the specimens during testing. The Krypton measuring system had its own data acquisition software, so the two sets of data were synchronized during post-processing. Once a specimen was secured in the testing frame, it was preloaded to about 225 lbs (1 kN) in the direction(s) of loading to remove any excess flexibility in the system and to ensure proper contact with the specimen.
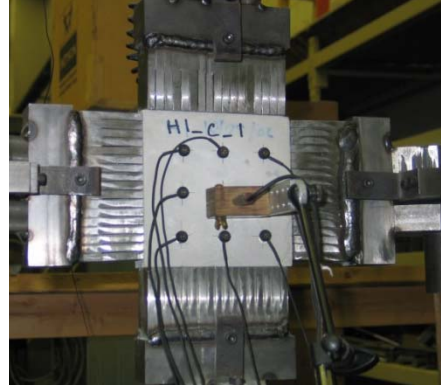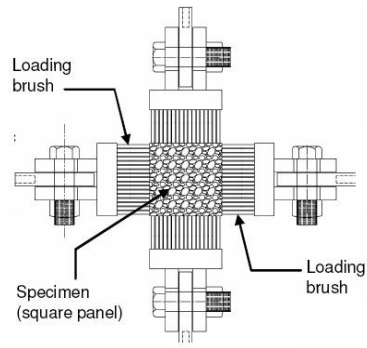
Figure 1.   Experimental test setup

Uniaxial Results

Failure Mode

To eventually better understand the response of the specimens under more complex biaxial stress states, the uniaxial failure mode and stress-strain response are first explored. Under uniaxial compression the failure modes exhibited by the plate specimens were similar to classical uniaxial plane concrete plate tests, with crack formation parallel to the axis of loading and perpendicular to the unloaded out-of-plane surface. Figure 2(a) shows the failure surface of a loaf NM6 plate specimen subjected to uniaxial compression, which was typical of specimens under similar loading.
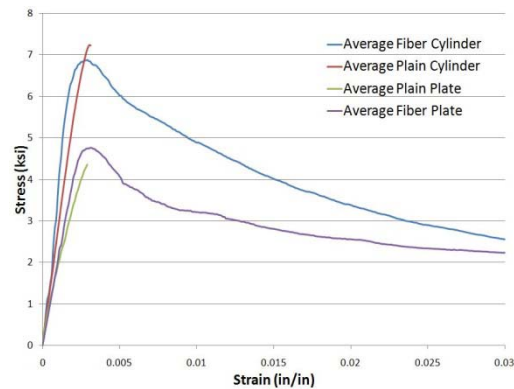

Figure 2.   Typical failure surface of uniaxial compression plate specimen (a), and NM6 uniaxial compressive behavior (b).

Since NM4 and NM6 were deliberately designed not to be high strength concrete mixes, crack formation and propagation occurred in the cementitious mortar (around the coarse aggregate). Crack formation was characterized by a series of vertical splitting cracks, which resulted in a dramatic loss of capacity for the plain concrete specimens; however, due to the passive confinement afforded by the fibers, the fiber-reinforced specimens still exhibited significant ductility beyond peak loading.

Stress-Strain Behavior

Due to the displacement-controlled nature of the experiments, loading was stable beyond the maximum load on the specimen, and the descending branch of the stress-strain curve was obtained out to fairly large deformations. Figure 2(b) shows a comparison of the average stress-strain response of NM6 HPFRCC and plain concrete results for both plate and cylinder specimens. It can be seen that the plain specimens failed abruptly, without any significant post-peak response; however, the HPFRCC exhibited a gradual descending branch and a sustained capacity of approximately 50% of the maximum applied load out to 3% strain. This significant deformation capacity is further evidence of the energy dissipating capability of the material. These average stress-strain curves were found by averaging the stress of the specimens for a given strain obtained from the Krypton LEDs. When processing the data, the flexibility in the experimental test setup was obtained by comparing the relationship between the stiffness found using data from the loading platens and that obtained from the Krypton targets. Since it is possible for local strain accumulation to negatively influence the data collected at individual LEDs on the surface of the specimen, once the flexibility in the test setup was corrected for in the experimental data, reliable post-peak behavior for the fiber-reinforced specimens was then able to be obtained from the actuators. Figure 2(b) also shows that the HPFRCC specimens were slightly stiffer than the plain concrete specimens as the loading increased, but the stiffnesses were almost identical up to 2 ksi (13.8 MPa). This change in stiffness can be attributed to the hooked steel fibers arresting the propagation and development of early cracking. Also, it can be seen that the average uniaxial strengths of the plain and HPFRCC specimens only slightly differed, which is consistent with the literature (Yin et al. 1989). With regard to varying the fiber volume fraction, previous test results on MM specimens showed the general trend that, as fiber volume fraction increased from 1 to 2 percent, the unconfined uniaxial compressive strength from cylinder tests slightly decreased (Foltz et al. 2008). Further, the maximum stress was achieved in both the cylinders and plate specimens under uniaxial compression at a strain of approximately 0.003 for both the plain and HPFRCC specimens. Figure 3(a) displays the results of direct uniaxial tension tests conducted on hooked fiber and plain MM specimens. It can be seen that the addition of fibers increased the tensile strength by greater than 500%, and the deformation capacity was also dramatically increased, with 50% of the peak tensile strength maintained to 1% strain. Finally, indirect tension tests were conducted on NM6 specimens, with similarly beneficial deformation and strength results observed in the fiber specimens.

Poisson's ratio was also investigated under uniaxial compression. During cylinder tests, the diametrical strain was obtained using a specially designed extensometer, while the longitudinal strain was obtained using a linear extensometer. The cylinder tests were also conducted using displacement-control, so the post-peak behavior was captured. Figure 3(b) shows the average longitudinal strain versus applied stress, as well as the average diametrical strain versus applied stress, for the NM6 cylinder tests. The diametrical strain measurement was limited to 0.01 due to the gage length of the extensometer.

Poisson's ratio was obtained from the initial portion of the stress-strain curve (applied stress of from 1 to 3 ksi) for each of the specimens. The lower bound for this calculation was selected to eliminate the potential for the seating of the specimen during experimentation to influence the result. Poisson's ratios for the plain and HPFRCC NM6 cylinders were found to be 0.24 and 0.22, respectively, while Poisson's ratios for the plain and HPFRCC NM6 plate

specimens were found to be 0.26 and 0.22, respectively. These results are consistent throughout the other mixes, as well as with typical values for uniaxially loaded plain concrete specimens (Kupfer et al. 1969).
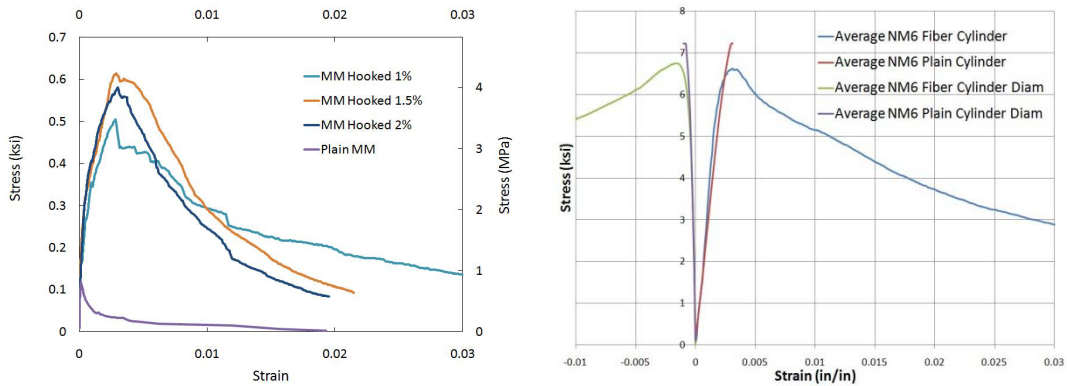

Figure 3.   Direct uniaxial tension test results for MM (a), and complete stress-strain curve for NM6 cylinder tests (b).

Biaxial Results

Failure Mode

The typical failure mechanism of the plain concrete specimens was by tensile splitting of the concrete. Under biaxial loading, the origination of a failure surface along a plane parallel to the plane of the test specimen resulted in an abrupt failure. However, the failure mechanisms experienced by the loaf fiber specimens under biaxial loading were considerably different.

Figure 4.   Single shear failure mode (a), and multiple shear failure mode (b), due to biaxial compressive loading; and typical RC coupling beam damage (c).

As described in previous research (Yin et al. 1989), these specimens experienced a faulting or shear failure due to the formation of multiple fault planes in the specimen. Similar to previous tests, all specimens exhibited either single shear or multiple shear failure modes (Ren et al. 2008). The single shear failure mode can be identified by a single diagonal crack inclined at about 30° to the unloaded out-of-plane surface, resulting in two triangularly shaped prisms. The multiple shear failure mode is similar to single shear, except the specimen fails along several

inclined diagonal cracks, resulting in it being divided into a few triangular pyramids. Figure 4 shows examples of both the single shear and multiple shear failure modes, as well as an illustration of typical damage experienced by RC coupling beams subjected to a seismic event.

Stress-Strain Behavior

The biaxial stress-strain behavior is largely dependent upon the ratio of applied axial loads. As previously described, the loading ratio was varied by altering the horizontal strain rate in the biaxial testing machine. Figure 5(a) shows the average compressive response of the leading direction of the biaxially loaded NM6 specimens. It can be seen that a similar peak stress was obtained for loading ratios of 0.5, 0.7, and 1.0. Also, significant residual strength was maintained to very large compressive strains; in fact, more than half of the peak strength was observed at strains as large as 3%. Figure 5(b) displays the average compressive response of the biaxially loaded NM6 in the trailing (horizontal) direction. (The uniaxial compressive response has been shown on both plots for reference.)
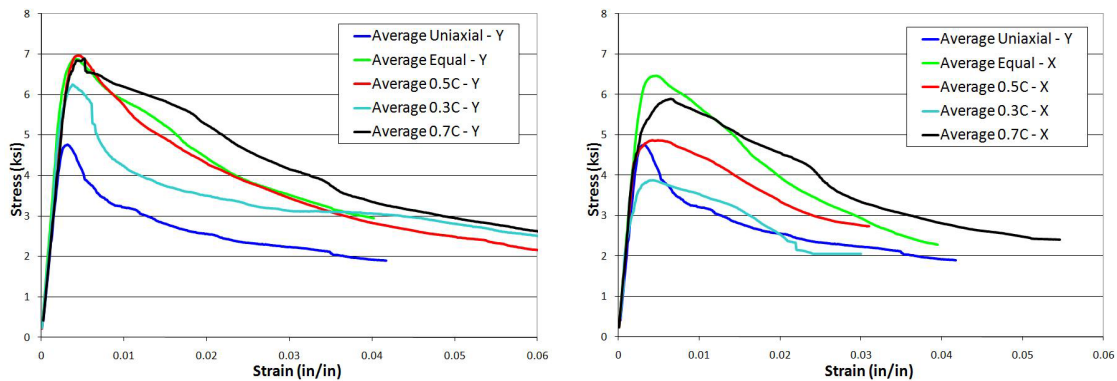

Figure 5. NM6 average compressive response in leading direction (a), and corresponding average compressive response in trailing direction (b).

The stiffness is essentially the same in both directions of loading, further indicating a thorough and random dispersion of fibers in the loaf specimens. Another observation is that biaxially loaded specimens at lower loading ratios, such as seen for 0.3, experienced earlier softening with respect to the applied strain in the trailing direction. This result can be attributed to the significant accumulation of damage in the leading direction during the test. Since the loadings in each direction were begun simultaneously, the specimen had undergone considerable deformation in the leading direction before obtaining a substantial strain in the trailing direction. Also, the strain at the maximum applied stress shifted to about 0.004 for specimens subjected to a biaxial loading ratio of 0.5 or greater, while the strain at the maximum stress was approximately 0.003 for the uniaxial specimens. Previous research shows the strain at the onset of significant spalling for short RC columns (analogous to coupling beams) occurs at about 0.005 (Berry and Eberhard 2003). Since HPFRCC specimens exhibit a residual strength of about 70% of the peak value at a strain of 0.01, the deformation capacity of HPFRCC can dramatically improve the seismic performance of such structural elements.

Failure Envelope

Non-dimensionalized ultimate strength data are shown as biaxial stress envelopes,

depicted in Figure 6. Stresses are reported as fractions of the average unconfined uniaxial compressive plate strength of the specimens for the particular concrete mixture and fiber volume fraction, σ_{co}. (Average uniaxial compressive plate strengths are given in Table 1.) Figure 6(a) shows the biaxial failure envelopes obtained from this testing program. This figure illustrates the effect of a more random fiber orientation by plotting the average result for each tested type of fiber, concrete mixture, and specimen (loaf vs. individually cast). The averaged curves were obtained by first normalizing each specific concrete batch by its average uniaxial value, and then the data points that had a similar failure stress ratio for a particular specimen, mix, and fiber type were averaged to create the data points for the curve. For example, the average loaf Spectra curve was made by first normalizing the 1.0, 1.5, and 2.0 percent fiber volume fraction results by their respective average uniaxial values, and then data points with similar failure stress ratios were averaged together. Each plot has been normalized by its average uniaxial compressive performance, so the individual specimens were not actually weaker than the loaf specimens; they just did not benefit as much from the addition of a second principal confining stress. All of the loaf specimens (hooked, Spectra, and NM6) experienced a much greater benefit under biaxial loading due to the passive confinement provided by the randomly oriented fibers; in fact, a strength increase of greater than 40 percent more than their respective uniaxial strengths under equal biaxial loading was observed.
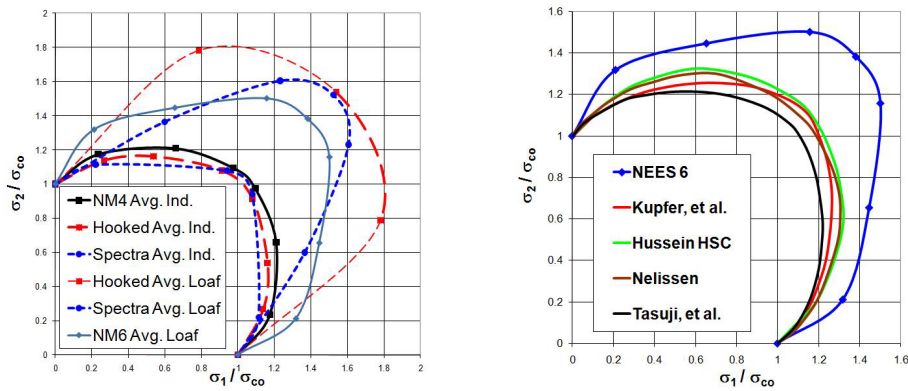

Figure 6.   Biaxial strength envelopes from experimental test results (a), and comparison of NM6 specimens with historical tests (b).

In Figure 6(b), a comparison of the average NM6 loaf specimen results with those obtained by other experiments from the literature on plain concrete is shown (Kupfer et al. 1969; Hussein and Marzouk 2000; Nelissen 1972; and Tasuji et al. 1978). It can be seen that the benefit of a biaxial stress state on the strength of the concrete is markedly increased with the addition of fibers in the HPFRCC specimens.

Conclusions

Results from an experimental investigation on HPFRCC indicate that it has many possibilities as an energy-dissipating material for structural elements susceptible to seismic events. The inclusion of either Spectra (polyethylene) or hooked steel fibers greatly increases the biaxial compressive strength of the concrete, as well as having a dramatic effect on the ductility of the material. The results have shown that under biaxial compression, the residual strength of the material was above 50 percent of the maximum stress at as large as 2 percent strains. While the experimental study undertaken did not explicitly investigate the cyclic

behavior of the specimens, understanding the monotonic nonlinear behavior of HPFRCC under complicated stress states is a significant step toward capturing the envelope response of the material. Future completion of tension tests will further the understanding of the behavior of this sort of HPFRCC and provide more comprehensive knowledge about the material and its full biaxial behavior. Such thorough understanding of HPFRCC has many implications, including making computer modeling and extension of the material's use to more large-scale structural applications possible. Combining the knowledge and behavioral trends gained through laboratory tests of HPFRCC materials with the vast coupling beam experimental information already available in the literature, it should be possible to redefine the design and performance of coupled wall systems for seismic applications.

Acknowledgments

References

Canbolat, B. A., Parra-Montesinos, G. J. and Wight, J. K., 2005. Experimental Study on Seismic Behavior of High-Performance Fiber-Reinforced Cement Composite Coupling Beams, *ACI Structural Journal* 102 (1), 159-166.

Berry, M. and Eberhard, M., 2003. Performance Models for Flexural Damage in Reinforced Concrete Columns, Pacific Earthquake Engineering Research Center Report 18, 162 pp.

Foltz, R.R., Guerra, J.M., and LaFave, J.M., 2008. Behavior of High-Performance Fiber-Reinforced Cementitious Composites for RC Coupling Beams in Earthquake-Resistant Structural Wall Systems, 14th World Conference on Earthquake Engineering, Beijing, China, October 2008.

Hussein, A. and Marzouk, H., 2000. Behavior of High Strength Concrete under Biaxial Stresses. *ACI Materials Journal* 97 (1), 27-36.

Kupfer, H., Hilsdorf, H.K., and Rusch, H., 1969. Behavior of Concrete under Biaxial Stresses, *ACI Journal Proceedings* 66 (8), 656-666.

Liao, W., Chao, S., Park, S., and Naaman, A.E., 2006. Self-Consolidating High Performance Fiber Reinforced Concrete (SCHPFRC) – Preliminary Investigation, *UMCEE 06-02*, 68 pp.

Nelissen, L.J., 1972. Biaxial Testing of Normal Concrete, *Heron* 18 (1), 90 pp.

Parra-Montesinos, G.J., 2005. High-Performance Fiber-Reinforced Cement Composites: An Alternative for Seismic Design of Structures, *ACI Structural Journal* 102 (5), 668-675.

Tasuji, M.E., Slate, F. O., and Nilsson, A. H., 1978. Stress-Strain Response and Fracture of Concrete in Biaxial Loading, *ACI Journal Proceedings* 75 (7), 306-312.

Ren, X., Yang, W., Zhou, Y., and Li, J., 2008. Behavior of High-Performance Concrete under Uniaxial and Biaxial Loading, *ACI Materials Journal* 105 (6), 548-557.

Yin, W., Su, E., Mansour, M., and Hsu, T., 1989. Biaxial Tests of Plain and Fiber Concrete. *ACI Materials Journal* 86 (3), 236-243.